46th AIAA/ASME/SAE/ASEE Joint Propulsion Conference & Exhibit
25 - 28 July 2010, Nashville, TN

AIAA 2010-7077

On the Compressible Hart-McClure Mean Flow Motion in Simulated Rocket Motors

Brian A. Maicke* and Joseph Majdalani†
University of Tennessee Space Institute, Tullahoma, TN 37388

We consider the compressible flow analogue of the solution known colloquially as the Hart-McClure profile. This potential motion is used to describe the mean flow in the original energy-based combustion instability framework. In this study, we employ the axisymmetric compressible form of the potential equation for steady, inviscid, irrotational flow assuming uniform injection of a calorically perfect gas in a porous, right-cylindrical chamber. This equation is expanded to order M_w^4 using a Rayleigh-Janzen sequence in powers of M_w^2, where M_w is the wall Mach number. At leading order, we readily recover the original Hart-McClure profile and, at M_w^2, a closed-form representation of the compressible correction. In view of the favorable convergence properties of the Rayleigh-Janzen expansion, the resulting approximation can be relied upon from the headwall down to the sonic point and slightly beyond in a long porous tube or nozzleless chamber. Based on the simple closed-form expressions that prescribe this motion, the principal flow attributes are quantified parametrically and compared to existing incompressible and one-dimensional theories. In this effort, the local Mach number and pressure are calculated and shown to provide an improved formulation when gauged against one-dimensional theory. Our results are also compared to the two-dimensional axisymmetric solution obtained by Majdalani (Majdalani, J., "On Steady Rotational High Speed Flows: The Compressible Taylor-Culick Profile," Proceedings of the Royal Society of London, Series A, Vol. 463, No. 2077, 2007, pp. 131-162). After rescaling the axial coordinate by the critical length L_s, a parametrically-free form is obtained that is essentially independent of the Mach number. This behavior is verified analytically, thus confirming Majdalani's universal similarity with respect to the critical distance. A secondary verification by computational fluid dynamics is also undertaken. When compared to existing rotational models, the compressible Hart-McClure plug-flow requires, as it should, a slightly longer distance to reach the speed of sound at the centerline. At that point, however, the entire cross-section is fully choked.

Nomenclature

a	=	chamber radius
c_0	=	stagnation speed of sound at chamber origin, $c_0 = \sqrt{\gamma p_0 / \rho_0}$
L_s	=	critical length or distance to the sonic point
M_w	=	wall Mach number
p	=	pressure normalized by headwall condition, $\bar{p} / p_0$
r, z	=	normalized radial and streamwise coordinates, $\bar{r} / a$, $\bar{z} / a$
U_c	=	centerline speed at headwall, $\bar{u}_z(0,0)$
U_w	=	wall injection velocity, $-\bar{u}_r(a,\bar{z})$
$\boldsymbol{u}$	=	normalized velocity $(\bar{u}_r, \bar{u}_z)/U_w$
u_c	=	normalized centerline speed at headwall, U_c / U_w
α	=	pure constant
ϕ	=	potential function

*Graduate Research Assistant, Mechanical, Aerospace and Biomedical Engineering Department. Member AIAA.
†H. H. Arnold Chair of Excellence in Advanced Propulsion, Mechanical, Aerospace and Biomedical Engineering Department. Senior Member AIAA. Fellow ASME.

Copyright © 2010 by B. A. Maicke and J. Majdalani. Published by the American Institute of Aeronautics and Astronautics, Inc., with permission.

λ = function of γ
μ , ρ = dynamic viscosity and density, μ, ρ
ψ = streamfunction

Subscripts and Symbols
0 = stagnation reference value
0 , 1 = leading or first order
c , s = centerline or sonic condition
$\underline{w}$ = sidewall condition in the gas
= dimensional variable

I. Introduction

DESPITE the preponderance of potential solutions for describing various conceivable motions in external and internal aerodynamics, a review of the literature surprisingly reveals a dearth of analytical models that have been rightfully extended to high speed settings where compressibility emerges as a major contributor. Hill's 1894 spherical vortex[1] constitutes one such example that had to linger over a century before receiving attention in Moore and Pullin's compressible flow analysis in 1998.[2] In fact, it may be safely argued that the scarcity of closed-form compressible models is not only germane to potential motions insofar as rotational problems share a similar disposition. The shortage of mathematical formulations associated with bounded fluids is even more substantial, as alluded to in recent articles on the subject.[3,4]

The development of a compressible rotational or irrotational solution is not only relevant in the context in which it appears, such as to better understand a mechanism or predict its general characteristics, but more importantly perhaps, it serves to provide the much needed benchmarks that are required to verify codes or test new theoretical concepts in the field, such as Kelvin's theorem for open regions,[5,6] and thereby help to advance the mathematical foundations of fluid mechanics in general, and compressible flow theory in particular. This can be seen in a study by Saad and Majdalani[6] who, in their effort at extending Kelvin's minimum energy theorem, canvassed the literature in search for multidimensional solutions that could pose as testbeds for the treatment of ducted fluids with open boundaries. While incompressible solutions could be located with relative ease, the identification of compressible flow profiles with suitable characteristics proved far more entreating.

Along similar lines, Wasistho, Balachandar and Moser[7] have argued that analytical representations can become an extraordinary resource for verifying numerical simulations in rocket motors. This is partly due to the challenges entailed in acquiring specific experimental measurements and, partly, as a consequence of the harsh environment developed in rocket chambers. In the same article, Wasistho *et al*.[7] suggest the use of a compressible mean flow profile in hydrodynamic instability calculations because of the heightened sensitivity displayed by their solutions on the base flow description. Their steady and unsteady results are subsequently compared to predictions derived from an integral formulation and, for the unsteady part, from a time-dependent expression for the oscillatory field by Majdalani and Van Moorhem.[8] Evidently, the favorable agreement and verification avenues reported by these researchers were contingent on the availability of reliable approximations.

This dichotomy in modeling approaches is only exacerbated with the advent of computer simulations. These are so heavily relied upon today that they have nearly superseded and fully replaced the formerly adopted methodologies. By way of example, the problem of simulating the internal mean flow in solid rocket motors has prompted several investigators within the propulsion community either to utilize Navier-Stokes solvers, such as Wasistho, Balachandar and Moser,[7] Chedevergne, Casalis and Majdalani,[9] Venugopal, Moser and Najjar,[10] Beddini,[11] Sabnis, Gibeling and McDonald,[12] Liou and Lien,[13] or to pursue simplified integral formulations that can be evaluated numerically, such as Traineau, Hervat and Kuentzmann,[14] Balakrishnan, Liñan and Williams,[15,16] Akiki and Majdalani,[17] and others. But as far as the analytical modeling of the compressible base flow is concerned, a rather limited number of studies may be cited, and these comprise, besides the authors,[3,4] work by Gany and Aharon.[18] The motivation for additional exploratory studies is clear. While reasons for this reduced emphasis may vary, they certainly include the mathematical challenges that arise in modeling compressible motions and the limited tools available for that purpose. In their compressible analysis of the porous channel flow, Maicke and Majdalani[4] provide an exposition of available numerical and analytical strategies, including those no longer in use, with special accent on the Rayleigh-Janzen expansion technique that will play a central role in this study.

Shifting attention to the steady-state velocity description in simulated rocket motors and porous tubes, several formulations have been systematically developed under incompressible, non-reactive chamber conditions. Examples include the irrotational model by McClure, Hart and Cantrell,[19] colloquially known as the Hart-McClure profile,[5] and the rotational equivalent by Taylor[20] and Culick,[21] often referred to as the Taylor-Culick mean flow. Following this tradition, other relevant models have been produced and these may be attributed to: Yuan and Finkelstein[22] who accounted for small viscosity, Majdalani and Saad[23] who accommodated arbitrary headwall injection and the effects of energy accumulation,[5] Sams *et al*.[24] and Kurdyumov[25] who incorporated the effects of wall taper and irregular cross-sections, and Majdalani *et al*.,[26,27] Zhou and Majdalani,[28] and Xu *et al*.[29] who allowed for time-dependent wall regression. Yet for those two-dimensional models in which compressibility is retained, a much shorter list may be identified. The one we find chiefly consists of the compressible Taylor-Culick flow analogue in porous tubes,[3] and the equivalent solution in porous channels.[4]

Given the above-mentioned paradigm, it is the purpose of this study to pursue a compressible mean flow approximation corresponding to the Hart-McClure profile. Although simple in its inception,[30] this model has played a key role in furthering the application of the energy balance method in a judiciously posed acoustic instability framework. Such a framework was carefully conceived by Hart, McClure and co-workers in a number of classic investigations featuring, to name a few: Hart and McClure,[31,32] McClure, Hart and Bird,[33] Cantrell, Hart and McClure,[34] Hart and Cantrell,[35] McClure, Hart and Cantrell,[19] Cantrell and Hart,[36] and Hart *et al*.[37] In fact, the energy-based methodology stands at the foundation of combustion instability analyses such as those undertaken by Flandro and Majdalani,[38] Fischbach, Majdalani and Flandro,[39] Majdalani, Flandro and Fischbach,[40] Majdalani, Fischbach and Flandro,[41] and Flandro, Fischbach and Majdalani.[42] One particular feature in the Hart-McClure injection pattern is the relaxation of the strictly radial velocity requirement at the sidewall. Such an assumption can prove helpful in the modeling of hybrid propellant rockets wherein a diffusion flame is established. It will also facilitate the modeling of the thermal boundary layer in the presence of a simplified, albeit pseudo two-dimensional, mean flow expression. The linearized equations associated with this model can prove instrumental in leveraging the method of superposition while seeking to accommodate irregular boundary conditions. Finally, given the growing emphasis on slip-boundary research in microfluidic systems and high speed applications, the quest for a compressible potential solution may viewed as a worthy endeavor in its own right.

The paper is organized as follows. We begin by revisiting the Hart-McClure problem in an axisymmetric, constant diameter chamber with uniform and non-orthogonal wall injection. Then using a Rayleigh-Janzen series in even powers of the wall Mach number, we expand the compressible potential equation up to fourth order and extract the compressible flow analogue of Hart-McClure's. Our analytical expression is then compared to one-dimensional theory, to its rotational counterpart, and to numerical simulations carried out under realistic turbulent conditions.

II. Mathematical Model

A. Geometry

We consider the steady, inviscid and non-heat conducting flow of an ideal gas in the domain bounded by the porous sidewall of a tube of radius a and finite length L_0. It is assumed that the non-orthogonal incoming speed of the gas at the wall has a radial component U_w and that L_0 can be sufficiently long to trigger sonic conditions. In solid and hybrid rockets, the sidewall velocity $U_w = \rho_P \dot{r}_P / \rho$ may be connected to the solid or fuel propellant regression rate, $\dot{r}_P$. To justify a constant U_w, we speculate that the streamwise depreciation in pressure and its wall-coupling effect can nearly offset the axial decrease in density. As shown in Fig. 1, $\bar{r}$ and $\bar{z}$ represent the radial and streamwise coordinates using a nomenclature in which the overbars denote dimensional quantities. All spatial variables are normalized by a in a coordinate system that has its origin at the headwall center. As usual, axial symmetry reduces the field investigation to the region $0 \le r \le 1$ and $0 \le z \le L$, where $L = L_0 / a$ stands for the aspect ratio. The tube can be taken to be closed at $z = 0$, corresponding to an inert headwall, and a sidewall velocity that conforms to the Hart-McClure profile (Fig. 1a). This configuration will be the main focus here with a slip-boundary at the sidewall. However, it is also possible to superimpose a headwall injection profile at $z = 0$ with characteristic speed U_c. The equivalent Taylor-Culick mean flow is illustrated in Fig. 1b where the orthogonality of the injected fluid is showcased. The incompressible model of this problem was treated by Majdalani and Saad,[23] whereas the compressible flow analogue was analyzed by Majdalani.[3] The resulting streamlines can be either induced by the injection process or by the two converging streams. The flowfield with headwall injection may be useful in modeling the bulk gaseous motion in hybrid rockets where U_w can be appreciably smaller than the

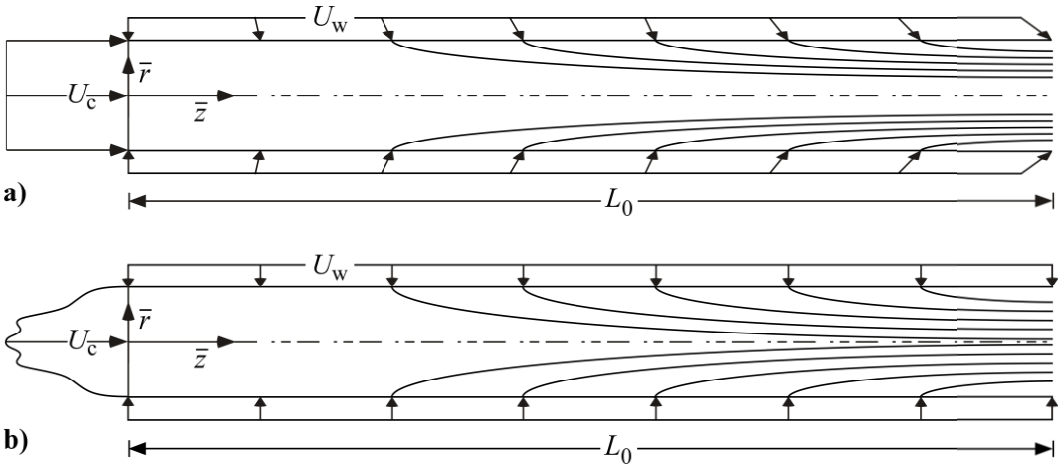

Figure 1. Schematic of a porous tube with a transpiring sidewall along which flow can enter in accordance with a) the Hart-McClure and b) Taylor-Culick injection profiles. Headwall injection is left arbitrary.

average velocity of the oxidizer stream, U_c. Typical hybrids exhibit values of $U_c/U_w \sim O(10^2 - 10^3)$ and $M_w = U_w/c_0 \sim O(10^{-4})$, where c_0 is the speed of sound at the origin. In seeking an exact potential solution in the Hart-McClure case, it is necessary for the headwall injection velocity to be irrotational and, therefore, invariant in the radial direction (i.e., uniform). Otherwise, only an approximate result may be obtained, as shown by Majdalani and Saad[23] in their rotational analysis of this problem with arbitrary headwall injection. In what follows, the steps leading to an exact potential solution will be delineated, although the addition of a secondary stream at the headwall can be readily considered by way of superposition.

B. Nomenclature and Boundary Conditions

We begin by normalizing the fundamental flow variables and operators using standard axisymmetric descriptors. These can be written as

$$u_r = \frac{\bar{u}_r}{U_w};\ u_z = \frac{\bar{u}_z}{U_w};\ p = \frac{\bar{p}}{p_0};\ T = \frac{\bar{T}}{T_0};\ \rho = \frac{\bar{\rho}}{\rho_0};\ \phi = \frac{\bar{\phi}}{aU_w};\ \psi = \frac{\bar{\psi}}{a^2 U_w};\ \boldsymbol{\Omega} = \frac{\bar{\boldsymbol{\Omega}} a}{U_w};\ \nabla = a\bar{\nabla};\ \mathrm{D}^2 = a^2\bar{\mathrm{D}}^2 \tag{1}$$

where ϕ, ψ, and $\boldsymbol{\Omega}$ denote the potential function, stream function, and vorticity, respectively. The latter may be referenced in connection with the Taylor-Culick model. The subscript '0' refers to conditions at the origin; $U_c = \bar{u}_z(0,0)$ and $U_w = -\bar{u}_r(a,\bar{z})$ define the injection constants along the headwall and sidewall, respectively. We also employ the second order Stokes operator D^2,

$$\mathrm{D}^2 \equiv \frac{\partial^2}{\partial r^2} - \frac{1}{r}\frac{\partial}{\partial r} + \frac{\partial^2}{\partial z^2} = r\frac{\partial}{\partial r}\left(\frac{1}{r}\frac{\partial}{\partial r}\right) + \frac{\partial^2}{\partial z^2} \tag{2}$$

As usual, the velocity, Stokes streamfunction, and potential function are related by

$$\boldsymbol{u} = u_r\boldsymbol{e}_r + u_z\boldsymbol{e}_z = \frac{\partial\phi}{\partial r}\boldsymbol{e}_r + \frac{\partial\phi}{\partial z}\boldsymbol{e}_z = -\frac{1}{\rho r}\frac{\partial\psi}{\partial z}\boldsymbol{e}_r + \frac{1}{\rho r}\frac{\partial\psi}{\partial r}\boldsymbol{e}_z \tag{3}$$

Given an isentropic flow of a calorically perfect gas with $\gamma \equiv c_p/c_v$, one also has

$$\rho = p^{1/\gamma} \text{ and } T = p^{1-1/\gamma} \tag{4}$$

Our auxiliary conditions are prescribed by the continuity of the flow across the centerline and radial inflow conditions at the sidewall that are consistent with both the Hart-McClure and Taylor-Culick representations. Headwall injection can be imposed on the streamwise component in the event of an open boundary. In adherence to the original Hart-McClure model, we begin by considering the case of no flow at $z = 0$. This assortment of conditions can be expressed by

$$\begin{cases} \bar{r}=0,\ \forall \bar{z},\ \bar{u}_r=0 & \text{(no flow across centerline)} \\ \bar{r}=a,\ \bar{z}=0,\ \bar{\phi}=0 & \text{(datum for potential flow)} \\ \bar{r}=a,\ 0\le \bar{z}<L_0,\ \bar{u}_r=-U_{\mathrm{w}} & \text{(uniform sidewall injection)} \\ \bar{z}=0,\ \forall \bar{r},\ \bar{u}_z=0 & \text{(no headwall injection)} \end{cases} \quad \text{and so} \quad \begin{cases} u_r(0,z)=\dfrac{\partial \phi(0,z)}{\partial r}=0 \\ \phi(0,0)=0 \\ u_r(1,z)=\dfrac{\partial \phi(1,z)}{\partial r}=-1 \\ u_z(r,0)=\dfrac{\partial \phi(r,0)}{\partial z}=0 \end{cases} \tag{5}$$

A solution that satisfies Eq. (5) may now be derived from the compressible form of the potential equation and then substituted back into the momentum equation so that the pressure is deduced. Isentropic relations will then be employed to calculate the density and temperature.

C. Potential Flow Equation

To derive the potential flow equation we begin with the continuity equation for cylindrical coordinates written in dimensional variables:

$$\frac{\partial}{\partial \bar{r}}\left(\bar{\rho}\bar{u}_r\bar{r}\right)+\frac{\partial}{\partial \bar{\theta}}\left(\bar{\rho}\bar{u}_\theta\right)+\bar{r}\frac{\partial}{\partial \bar{z}}\left(\bar{\rho}\bar{u}_z\right)=0 \tag{6}$$

To simplify matters, the tangential derivative is eliminated for axisymmetric motion. The result is an expanded version of Eq. (6) with

$$\bar{r}\left[\bar{u}_r\frac{\partial \bar{\rho}}{\partial \bar{r}}+\bar{u}_z\frac{\partial \bar{\rho}}{\partial \bar{z}}+\bar{\rho}\left(\frac{\partial \bar{u}_r}{\partial \bar{r}}+\frac{\partial \bar{u}_z}{\partial \bar{z}}\right)\right]+\bar{\rho}\bar{u}_r=0 \tag{7}$$

The potential functions are then introduced via

$$\bar{u}_r=\frac{\partial \bar{\phi}}{\partial \bar{r}} \quad \text{and} \quad \bar{u}_z=\frac{\partial \bar{\phi}}{\partial \bar{z}} \tag{8}$$

Substituting Eq. (8) into Eq. (7) yields

$$\bar{\rho}\left(\frac{\partial^2 \bar{\phi}}{\partial \bar{r}^2}+\frac{1}{\bar{r}}\frac{\partial \bar{\phi}}{\partial \bar{r}}+\frac{\partial^2 \bar{\phi}}{\partial \bar{z}^2}\right)=-\frac{\partial \bar{\phi}}{\partial \bar{r}}\frac{\partial \bar{\rho}}{\partial \bar{r}}-\frac{\partial \bar{\phi}}{\partial \bar{z}}\frac{\partial \bar{\rho}}{\partial \bar{z}} \tag{9}$$

The density terms must be eliminated to reach the desired potential equation. To that end, we invoke

$$\mathrm{d}\bar{p}=-\frac{\bar{\rho}}{2}\mathrm{d}\left[\left(\frac{\partial \bar{\phi}}{\partial \bar{r}}\right)^2+\left(\frac{\partial \bar{\phi}}{\partial \bar{z}}\right)^2\right] \tag{10}$$

Equation (10) represents Euler's equation in axisymmetric cylindrical coordinates. Recalling that the flow is isentropic, it is possible to express the speed of sound as

$$c^2=\frac{\mathrm{d}\bar{p}}{\mathrm{d}\bar{\rho}} \quad \text{or} \quad \mathrm{d}\bar{\rho}=\frac{\mathrm{d}\bar{p}}{c^2} \tag{11}$$

Here c is the local speed of sound and not a reference value. Equation (11) provides the means for eliminating the density from Eq. (9). This can be seen by combining Eqs. (10) and (11) into

$$\mathrm{d}\bar{\rho}=-\frac{\bar{\rho}}{2c^2}\mathrm{d}\left[\left(\frac{\partial \bar{\phi}}{\partial \bar{r}}\right)^2+\left(\frac{\partial \bar{\phi}}{\partial \bar{z}}\right)^2\right] \tag{12}$$

or

$$\frac{\partial \bar{\rho}}{\partial \bar{r}}\mathrm{d}\bar{r}+\frac{\partial \bar{\rho}}{\partial \bar{z}}\mathrm{d}\bar{z}=-\frac{\bar{\rho}}{2c^2}\left[2\frac{\partial \bar{\phi}}{\partial \bar{r}}\frac{\partial}{\partial \bar{r}}\left(\frac{\partial \bar{\phi}}{\partial \bar{r}}\right)\mathrm{d}\bar{r}+2\frac{\partial \bar{\phi}}{\partial \bar{r}}\frac{\partial}{\partial \bar{z}}\left(\frac{\partial \bar{\phi}}{\partial \bar{r}}\right)\mathrm{d}\bar{z}+2\frac{\partial \bar{\phi}}{\partial \bar{z}}\frac{\partial}{\partial \bar{r}}\left(\frac{\partial \bar{\phi}}{\partial \bar{z}}\right)\mathrm{d}\bar{r}+2\frac{\partial \bar{\phi}}{\partial \bar{z}}\frac{\partial}{\partial \bar{z}}\left(\frac{\partial \bar{\phi}}{\partial \bar{z}}\right)\mathrm{d}\bar{z}\right] \tag{13}$$

Collecting partial differentials in $\mathrm{d}\bar{r}$ and $\mathrm{d}\bar{z}$ and simplifying, we get

$$\begin{cases} \dfrac{\partial \bar{\rho}}{\partial \bar{r}}=-\dfrac{\bar{\rho}}{c^2}\left(\dfrac{\partial \bar{\phi}}{\partial \bar{r}}\dfrac{\partial^2 \bar{\phi}}{\partial \bar{r}^2}+\dfrac{\partial \bar{\phi}}{\partial \bar{z}}\dfrac{\partial^2 \bar{\phi}}{\partial \bar{r}\partial \bar{z}}\right) \\ \dfrac{\partial \bar{\rho}}{\partial \bar{z}}=-\dfrac{\rho}{c^2}\left(\dfrac{\partial \bar{\phi}}{\partial \bar{z}}\dfrac{\partial^2 \bar{\phi}}{\partial \bar{z}^2}+\dfrac{\partial \bar{\phi}}{\partial \bar{r}}\dfrac{\partial^2 \bar{\phi}}{\partial \bar{r}\partial \bar{z}}\right) \end{cases} \tag{14}$$

At this point, inserting Eq. (14) into Eq. (9) eliminates the density differentials and produces

$$\bar{\mathrm{D}}^2\bar{\phi} = \frac{1}{c^2}\left[\left(\frac{\partial\bar{\phi}}{\partial\bar{r}}\right)^2\frac{\partial^2\bar{\phi}}{\partial\bar{r}^2} + \left(\frac{\partial\bar{\phi}}{\partial\bar{z}}\right)^2\frac{\partial^2\bar{\phi}}{\partial\bar{z}^2} + 2\frac{\partial\bar{\phi}}{\partial\bar{r}}\frac{\partial\bar{\phi}}{\partial\bar{z}}\frac{\partial^2\bar{\phi}}{\partial\bar{r}\partial\bar{z}}\right] \tag{15}$$

Since c is a local speed of sound, it must be expanded to account for the implied velocity potentials that it contains. When expressed in terms of its stagnation value, we get

$$c^2 = c_0^2 - \frac{\gamma-1}{2}\left[\left(\frac{\partial\bar{\phi}}{\partial\bar{r}}\right)^2 + \left(\frac{\partial\bar{\phi}}{\partial\bar{z}}\right)^2\right] \tag{16}$$

where c_0 is the speed of sound at stagnation conditions, often taken at the inert headwall. Thusly, Eq. (15) becomes

$$\left\{1 - \frac{\gamma-1}{2c_0^2}\left[\left(\frac{\partial\bar{\phi}}{\partial\bar{r}}\right)^2 + \left(\frac{\partial\bar{\phi}}{\partial\bar{z}}\right)^2\right]\right\}\bar{\mathrm{D}}^2\bar{\phi} = \frac{1}{c_0^2}\left[\left(\frac{\partial\bar{\phi}}{\partial\bar{r}}\right)^2\frac{\partial^2\bar{\phi}}{\partial\bar{r}^2} + \left(\frac{\partial\bar{\phi}}{\partial\bar{z}}\right)^2\frac{\partial^2\bar{\phi}}{\partial\bar{z}^2} + 2\frac{\partial\bar{\phi}}{\partial\bar{r}}\frac{\partial\bar{\phi}}{\partial\bar{z}}\frac{\partial^2\bar{\phi}}{\partial\bar{r}\partial\bar{z}}\right] \tag{17}$$

Applying the normalization designated in Eq. (1) adds a U_w^2 term to the elements that are divided by c_0^2. This leaves us with the compressible, two-dimensional, axisymmetric form of the potential equation:

$$\left\{1 - M_\mathrm{w}^2\frac{\gamma-1}{2}\left[\left(\frac{\partial\phi}{\partial r}\right)^2 + \left(\frac{\partial\phi}{\partial z}\right)^2\right]\right\}\mathrm{D}^2\phi = M_\mathrm{w}^2\left[\left(\frac{\partial\phi}{\partial r}\right)^2\frac{\partial^2\phi}{\partial r^2} + \left(\frac{\partial\phi}{\partial z}\right)^2\frac{\partial^2\phi}{\partial z^2} + 2\frac{\partial\phi}{\partial r}\frac{\partial\phi}{\partial z}\frac{\partial^2\phi}{\partial r\partial z}\right] \tag{18}$$

III. Solution

A. Rayleigh-Janzen Expansion

The compressible potential flow equation[43] is subject to four boundary conditions associated with the Taylor-Culick irrotational flow, known colloquially as the Hart-McClure profile. These conditions correspond to: a) an impermeable headwall, b) no radial flow across the centerline, c) a radial sidewall velocity equal to the injection velocity, and d) a vanishing reference potential at the center of the headwall. Mathematically, we write

$$\frac{\partial\phi}{\partial z}(r,0) = 0; \quad \frac{\partial\phi}{\partial r}(0,z) = 0; \quad \frac{\partial\phi}{\partial r}(1,z) = -1; \quad \phi(0,0) = 0. \tag{19}$$

In retrospect, the above conditions are similar to those used by Culick[21] except for the no-slip requirement which is not needed here. Equation (18) may be rearranged into

$$\mathrm{D}^2\phi = M_\mathrm{w}^2\left\{\left(\frac{\partial\phi}{\partial r}\right)^2\frac{\partial^2\phi}{\partial r^2} + \left(\frac{\partial\phi}{\partial z}\right)^2\frac{\partial^2\phi}{\partial z^2} + 2\frac{\partial\phi}{\partial r}\frac{\partial\phi}{\partial z}\frac{\partial^2\phi}{\partial r\partial z} + \frac{\gamma-1}{2}\left[\left(\frac{\partial\phi}{\partial r}\right)^2 + \left(\frac{\partial\phi}{\partial z}\right)^2\right]\mathrm{D}^2\phi\right\} \tag{20}$$

At this stage, a Rayleigh-Janzen expansion in the square of the Mach number may be called upon. This expansion is based on

$$\phi(r,z) = \phi_0(r,z) + M_\mathrm{w}^2\phi_1(r,z) + O(M_\mathrm{w}^4) \tag{21}$$

Substituting Eq. (21) into Eq. (20) yields, after some cancellations,

$$\left(\frac{\partial^2\phi_0}{\partial r^2} + \frac{1}{r}\frac{\partial\phi_0}{\partial r} + \frac{\partial^2\phi_0}{\partial z^2}\right) + M_\mathrm{w}^2\left(\frac{\partial^2\phi_1}{\partial r^2} + \frac{1}{r}\frac{\partial\phi_1}{\partial r} + \frac{\partial^2\phi_1}{\partial z^2}\right)$$
$$= M_\mathrm{w}^2\left\{\left(\frac{\partial\phi_0}{\partial r}\right)^2\frac{\partial^2\phi_0}{\partial r^2} + \left(\frac{\partial\phi_0}{\partial z}\right)^2\frac{\partial^2\phi_0}{\partial z^2} + 2\frac{\partial\phi_0}{\partial r}\frac{\partial\phi_0}{\partial z}\frac{\partial^2\phi_0}{\partial r\partial z} + \frac{\gamma-1}{2}\left[\left(\frac{\partial\phi_0}{\partial r}\right)^2 + \left(\frac{\partial\phi_0}{\partial z}\right)^2\right]\mathrm{D}^2\phi_0\right\} \tag{22}$$

Similarly, to determine the thermodynamic variables, we can expand Eq. (10) using

$$\begin{cases} p(r,z) = 1 + M_\mathrm{w}^2 p_1(r,z) + M_\mathrm{w}^4 p_2(r,z) + O(M_\mathrm{w}^6) \\ \rho(r,z) = 1 + M_\mathrm{w}^2\rho_1(r,z) + M_\mathrm{w}^4\rho_2(r,z) + O(M_\mathrm{w}^6) \end{cases} \tag{23}$$

Then, substituting Eq. (23) into Eq. (10) engenders

$$\mathrm{d}\left(1 + M_\mathrm{w}^2 p_1 + M_\mathrm{w}^4 p_2\right) = -M_\mathrm{w}^2\left(\frac{1 + M_\mathrm{w}^2\rho_1 + M_\mathrm{w}^4\rho_2}{2}\right)\mathrm{d}\left\{\left[\frac{\partial\left(\phi_0 + M_\mathrm{w}^2\phi_1\right)}{\partial r}\right]^2 + \left[\frac{\partial\left(\phi_0 + M_\mathrm{w}^2\phi_1\right)}{\partial z}\right]^2\right\} \tag{24}$$

This relation will be expanded as needed to deduce the pressure at successive orders.

B. Leading-Order Solution

At $O(1)$, one identifies

$$\frac{\partial^2 \phi_0}{\partial r^2} + \frac{1}{r}\frac{\partial \phi_0}{\partial r} + \frac{\partial^2 \phi_0}{\partial z^2} = 0 \tag{25}$$

Then using $\phi_0(r,z) = f_0(r) + g_0(z)$, one obtains

$$\frac{\mathrm{d}^2 f_0}{\mathrm{d}r^2} + \frac{1}{r}\frac{\mathrm{d}f_0}{\mathrm{d}r} + \frac{\mathrm{d}^2 g_0}{\mathrm{d}z^2} = 0 \quad \text{or} \quad \frac{\mathrm{d}^2 f_0}{\mathrm{d}r^2} + \frac{1}{r}\frac{\mathrm{d}f_0}{\mathrm{d}r} = -\frac{\mathrm{d}^2 g_0}{\mathrm{d}z^2} \equiv \upsilon \tag{26}$$

where υ represents the separation constant. Integration in the two space coordinates can be carried out straightforwardly. One gets

$$\begin{cases} \dfrac{\mathrm{d}^2 f_0}{\mathrm{d}r^2} + \dfrac{1}{r}\dfrac{\mathrm{d}f_0}{\mathrm{d}r} = \upsilon; \quad f_0(r) = \frac{1}{4}\upsilon r^2 + C_1 \ln r + C_2 \\ -\dfrac{\mathrm{d}^2 g_0}{\mathrm{d}z^2} = \upsilon; \quad g_0(z) = -\frac{1}{2}\upsilon z^2 + C_3 z + C_4 \end{cases} \tag{27}$$

The boundary conditions can now be used to extract

$$\frac{\partial \phi_0(r,0)}{\partial z} = 0; \ \frac{\mathrm{d}g_0(0)}{\mathrm{d}z} = 0 \longrightarrow C_3 = 0 \tag{28}$$

$$\frac{\partial \phi_0(0,z)}{\partial r} = 0; \ \frac{\mathrm{d}f_0(0)}{\mathrm{d}r} = 0 \longrightarrow C_1 = 0 \tag{29}$$

$$\frac{\partial \phi_0(1,z)}{\partial r} = -1; \ \frac{\mathrm{d}f_0(1)}{\mathrm{d}r} = -1 \longrightarrow \upsilon = -2 \tag{30}$$

$$\phi_0(0,0) = 0; \ f_0(0) + g_0(0) = 0 \longrightarrow C_2 + C_4 = 0 \tag{31}$$

In total, we collect

$$f_0 = -\tfrac{1}{2}r^2 + C_2; \ g_0 = z^2 + C_4 \tag{32}$$

and so

$$\phi_0 = f_0 + g_0 = -\tfrac{1}{2}r^2 + z^2 + C_2 + C_4 \tag{33}$$

Then by virtue of Eq. (31), we are left with

$$\phi_0 = -\tfrac{1}{2}r^2 + z^2 \tag{34}$$

We thus recover the irrotational, incompressible, inviscid solution that is often referred to in the propulsion community as the Hart-McClure profile.[31,34,36] This profile was the precursor to Culick's model and constitutes one of the first base flows used to study combustion instability in solid rocket motors. Outside the realm of propulsion, the same solution is used to model flow around a cavity. Its velocity components are simply given by:

$$u_r = -r; \quad u_\theta = 0; \quad u_z = 2z \tag{35}$$

So while it satisfies mass conservation, it remains irrotational. The leading order pressure may be easily obtained from retaining the $O(M_\mathrm{w}^2)$ elements of Eq. (24), namely

$$\mathrm{d}p_1 = -\tfrac{1}{2}\gamma\,\mathrm{d}\left[\left(\frac{\partial \phi_0}{\partial r}\right)^2 + \left(\frac{\partial \phi_0}{\partial z}\right)^2\right] \tag{36}$$

Integration of Eq. (36) generates

$$p_1 = -\tfrac{1}{2}\gamma\left(r^2 + 4z^2\right) \quad \text{or} \quad p(r,z) = 1 - \tfrac{1}{2}\gamma\left(r^2 + 4z^2\right)M_\mathrm{w}^2 + O(M_\mathrm{w}^4) \tag{37}$$

Note that the constant of integration is nil according to the reference condition at the headwall.

C. First-Order Mach Number Correction

At $O(M_\mathrm{w}^2)$, we retrieve from Eq. (22),

$$\mathrm{D}^2\phi = \left(\frac{\partial \phi_0}{\partial r}\right)^2 \frac{\partial^2 \phi_0}{\partial r^2} + \left(\frac{\partial \phi_0}{\partial z}\right)^2 \frac{\partial^2 \phi_0}{\partial z^2} + 2\frac{\partial \phi_0}{\partial r}\frac{\partial \phi_0}{\partial z}\frac{\partial^2 \phi_0}{\partial r \partial z} + \frac{\gamma - 1}{2}\left[\left(\frac{\partial \phi_0}{\partial r}\right)^2 + \left(\frac{\partial \phi_0}{\partial z}\right)^2\right]\mathrm{D}^2\phi_0 \tag{38}$$

Equation (38) appears, at first glance, nearly intractable. However, it may be verified that the substitution of $\phi_0 = -\frac{1}{2}r^2 + z^2$ will prompt several major simplifications that leave us simply with

$$\frac{\partial^2 \phi_1}{\partial r^2} + \frac{1}{r}\frac{\partial \phi_1}{\partial r} + \frac{\partial^2 \phi_1}{\partial z^2} = -r^2 + 8z^2 \tag{39}$$

As before, we posit a separable solution of the type $\phi_1(r,z) = f_1(r) + g_1(z)$. The same process is then repeated, starting with

$$\frac{\mathrm{d}^2 f_1}{\mathrm{d}r^2} + \frac{1}{r}\frac{\mathrm{d}f_1}{\mathrm{d}r} + \frac{\mathrm{d}^2 g_1}{\mathrm{d}z^2} = -r^2 + 8z^2 \tag{40}$$

The radial and axial functions may be readily segregated by putting

$$\frac{\mathrm{d}^2 f_1}{\mathrm{d}r^2} + \frac{1}{r}\frac{\mathrm{d}f_1}{\mathrm{d}r} + r^2 = -\frac{\mathrm{d}^2 g_1}{\mathrm{d}z^2} + 8z^2 \equiv \kappa \tag{41}$$

where κ denotes the separation constant. On the one hand, the radial function becomes

$$\frac{\mathrm{d}^2 f_1}{\mathrm{d}r^2} + \frac{1}{r}\frac{\mathrm{d}f_1}{\mathrm{d}r} + r^2 = \kappa; \quad f_1(r) = \kappa\frac{r^2}{4} - \frac{r^4}{16} + K_1 \ln r + K_2 \tag{42}$$

On the other hand, we collect in the axial variable,

$$-\frac{\mathrm{d}^2 g_1}{\mathrm{d}z^2} + 8z^2 = \kappa; \quad g_1(z) = \frac{2}{3}z^4 - \frac{\kappa}{2}z^2 + K_3 z + K_4 \tag{43}$$

At this juncture, the boundary conditions may be applied to give:

$$\begin{cases} \dfrac{\partial \phi_1(r,0)}{\partial z} = 0; \quad \dfrac{\mathrm{d}g_1(0)}{\mathrm{d}z} = 0 \longrightarrow \quad K_3 = 0 \\ \dfrac{\partial \phi_1(0,z)}{\partial r} = 0; \quad \dfrac{\mathrm{d}f_1(0)}{\mathrm{d}r} = 0 \longrightarrow \quad K_1 = 0 \\ \dfrac{\partial \phi_1(1,z)}{\partial r} = 0; \quad \dfrac{\mathrm{d}f_1(1)}{\mathrm{d}r} = 0 \longrightarrow \quad \kappa = \dfrac{1}{2} \\ \phi_1(0,0) = 0; \quad f_1(0) + g_1(0) = 0 \longrightarrow \quad K_2 + K_4 = 0 \end{cases} \tag{44}$$

Backward substitution of these constants leads to

$$\phi_1(r,z) = \tfrac{1}{8}r^2 - \tfrac{1}{16}r^4 + \tfrac{2}{3}z^4 - \tfrac{1}{4}z^2 \tag{45}$$

At length, combining leading and first order contributions, we arrive at

$$\phi(r,z) = \phi_0 + M_\mathrm{w}^2\phi_1 + O(M_\mathrm{w}^4) = -\tfrac{1}{2}r^2 + z^2 + (\tfrac{1}{8}r^2 - \tfrac{1}{16}r^4 + \tfrac{2}{3}z^4 - \tfrac{1}{4}z^2)M_\mathrm{w}^2 + O(M_\mathrm{w}^4) \tag{46}$$

and so, finally,

$$\boxed{\phi(r,z) = -\tfrac{1}{2}r^2 + z^2 + \tfrac{1}{48}\left[3(2-r^2)r^2 + 4(8z^2-3)z^2\right]M_\mathrm{w}^2 + O(M_\mathrm{w}^4)} \tag{47}$$

Based on Eq. (47), the velocity and pressure fields may be derived, namely,

$$\boxed{\begin{cases} u_r = -r + \tfrac{1}{4}(1-r^2)rM_\mathrm{w}^2 + O(M_\mathrm{w}^4) \\ u_z = 2z + \tfrac{1}{6}(16z^2-3)zM_\mathrm{w}^2 + O(M_\mathrm{w}^4) \end{cases}} \tag{48}$$

To circumvent the introduction of the density in the $O(M_\mathrm{w}^4)$ Euler equation, we segregate the total differentials into their partial components via

$$\begin{cases} \dfrac{\partial p_2}{\partial r} = -\gamma\left[\rho_1\left(\dfrac{\partial \phi_0}{\partial r}\dfrac{\partial^2 \phi_0}{\partial r^2} + \dfrac{\partial \phi_0}{\partial z}\dfrac{\partial^2 \phi_0}{\partial r \partial z}\right) + \dfrac{\partial \phi_0}{\partial r}\dfrac{\partial^2 \phi_1}{\partial r^2} + \dfrac{\partial \phi_1}{\partial r}\dfrac{\partial^2 \phi_0}{\partial r^2} + \dfrac{\partial \phi_1}{\partial z}\dfrac{\partial^2 \phi_0}{\partial r \partial z} + \dfrac{\partial \phi_0}{\partial z}\dfrac{\partial^2 \phi_1}{\partial r \partial z}\right] \\ \dfrac{\partial p_2}{\partial z} = -\gamma\left[\rho_1\left(\dfrac{\partial \phi_0}{\partial z}\dfrac{\partial^2 \phi_0}{\partial z^2} + \dfrac{\partial \phi_0}{\partial r}\dfrac{\partial^2 \phi_0}{\partial r \partial z}\right) + \dfrac{\partial \phi_0}{\partial z}\dfrac{\partial^2 \phi_1}{\partial z^2} + \dfrac{\partial \phi_1}{\partial z}\dfrac{\partial^2 \phi_0}{\partial z^2} + \dfrac{\partial \phi_1}{\partial r}\dfrac{\partial^2 \phi_0}{\partial r \partial z} + \dfrac{\partial \phi_0}{\partial r}\dfrac{\partial^2 \phi_1}{\partial r \partial z}\right] \end{cases} \tag{49}$$

The nature of the potential solution precludes the existence of the mixed differential terms, simplifying Eq. (49) to

$$\begin{cases} \dfrac{\partial p_2}{\partial r} = -\gamma\left[\rho_1\left(\dfrac{\partial \phi_0}{\partial r}\dfrac{\partial^2 \phi_0}{\partial r^2}\right) + \dfrac{\partial \phi_0}{\partial r}\dfrac{\partial^2 \phi_1}{\partial r^2} + \dfrac{\partial \phi_1}{\partial r}\dfrac{\partial^2 \phi_0}{\partial r^2}\right] \\ \dfrac{\partial p_2}{\partial z} = -\gamma\left[\rho_1\left(\dfrac{\partial \phi_0}{\partial z}\dfrac{\partial^2 \phi_0}{\partial z^2}\right) + \dfrac{\partial \phi_0}{\partial z}\dfrac{\partial^2 \phi_1}{\partial z^2} + \dfrac{\partial \phi_1}{\partial z}\dfrac{\partial^2 \phi_0}{\partial z^2}\right] \end{cases} \tag{50}$$

Integration of Eq. (50) produces

$$\begin{cases} p_2 = -\gamma\left[\frac{1}{8}\left(r^4 - 2r^2\right) - r^2 z^2\right] + G(z) \\ p_2 = -\gamma\left[\frac{10}{3} z^4 - z^2 - r^2 z^2\right] + F(r) \end{cases} \tag{51}$$

The total pressure correction may then be deduced from the combined integrals of Eq. (51). Being an exact differential at each order, we get

$$p_2 = -\gamma\left[\frac{1}{8}\left(r^4 - 2r^2\right) - r^2 z^2 + \frac{10}{3} z^4 - z^2\right] \tag{52}$$

whence, by way of Eq. (23), we arrive at

$$\boxed{p(r,z) = 1 - \tfrac{1}{2}\gamma\left(r^2 + 4z^2\right) M_{\mathrm{w}}^2 - \gamma\left[\tfrac{1}{8}\left(r^4 - 2r^2\right) - r^2 z^2 + \tfrac{10}{3} z^4 - z^2\right] M_{\mathrm{w}}^4 + O(M_{\mathrm{w}}^6)} \tag{53}$$

IV. Results and Discussion

A. Potential Lines

Figure 2 shows the potential lines for a reference case of $M_{\mathrm{w}} = 0.01$. In Fig. 2a the effects of compressibility are presented as a leftward shift of the potential lines. There is very little change in curvature for the potential lines as the flow in the downstream region is predominantly axial. Figure 2b shows a more detailed view of the potential lines near the head end of the chamber. Here, the axial and radial velocities are of the same order, resulting in increased curvature of the potential lines. The diagonal crossing the origin demarcates the border between radial and axial dominance of the flow. As expected, the compressibility effects in this region are virtually nonexistent as the compressible and incompressible potential lines are directly on top of each other.

B. Critical Length and Universal Similarity

Characterizing the critical length, also called the sonic length, is an integral measure to compare the present study to existing experimental and computational data. By normalizing the length of a motor by the critical length, it is possible to compare the analytical predictions directly to numerical or experimental data, provided the choking length is known. Past solutions have also displayed similarity behavior when normalized by the critical length in so far as the solution is weakly dependent on the Mach number. This similarity is especially useful when weighing multiple models against each other as only a single Mach number is necessary for a complete comparison. With this in mind, we examine the dimensional quantities

$$\frac{\bar{u}_z}{c} = 1 \tag{54}$$

Equation (54) provides the criterion for the critical length. When the dimensional axial velocity divided by the local speed of sound reaches unity, the choking condition is satisfied. Rewriting Eq. (54) in terms of our dimensionless solution and squaring both sides, we have

$$\frac{u_z^2}{T}\frac{U_{\mathrm{w}}^2}{T_0 R\gamma} = 1 \tag{55}$$

The reference constants may be collected to retrieve

$$M_{\mathrm{w}}^2 u_z^2 = T \tag{56}$$

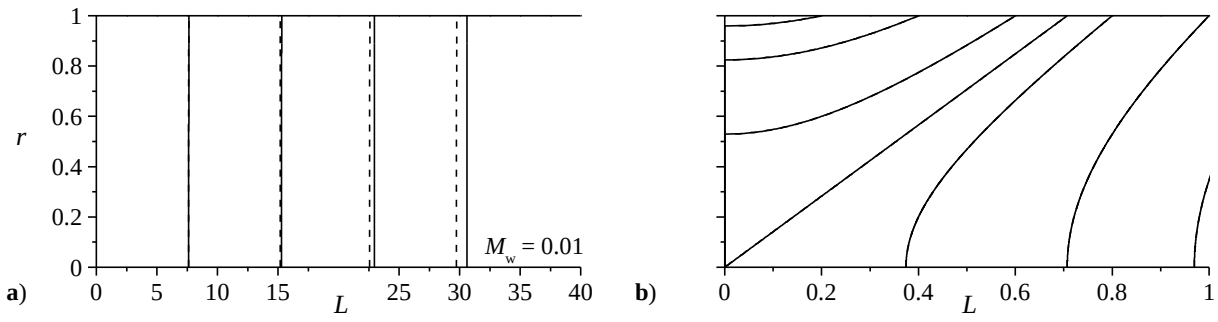

Figure 2. Potential lines for the compressible (dashed) and incompressible solutions (solid) using M_{w}=0.01.

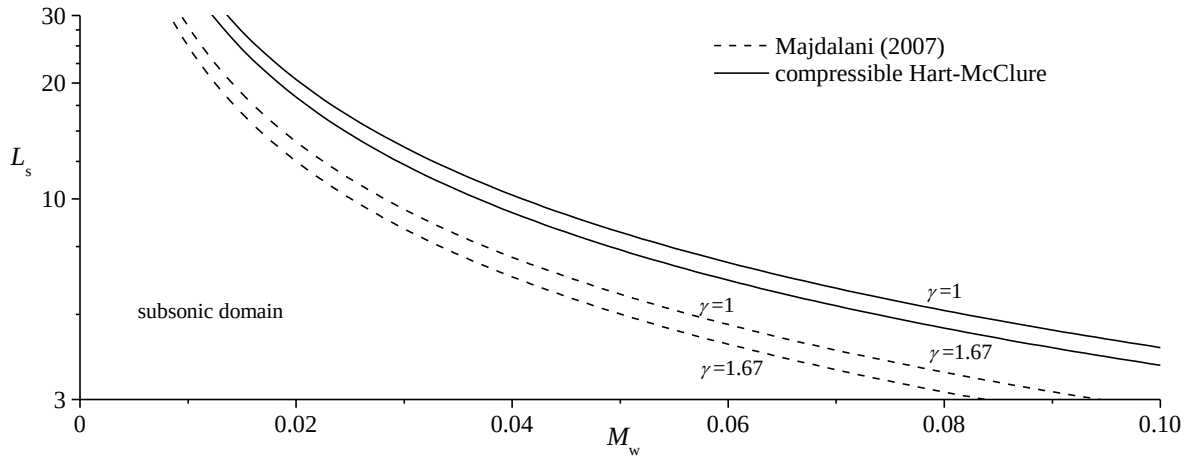

Figure 3. Critical length over a range of injection Mach numbers.

At this juncture, we may insert the Rayleigh-Janzen expansion into Eq. (56) to obtain

$$M_w^2\left(\frac{\partial \phi_0}{\partial z}\right)^2 + M_w^4\left(\frac{\partial \phi_1}{\partial z}\right)^2 = 1 + M_w^2 T_1 + M_w^4 T_2 \tag{57}$$

Expanding Eq. (57) and ignoring the slight radial dependence, we find

$$4z^2M_w^2 + 4z(\tfrac{8}{3}z^3 - \tfrac{1}{2}z)M_w^4 + \left(\tfrac{8}{3}z^3 - \tfrac{1}{2}z\right)^2 M_w^6 = 1 - 2(\gamma-1)z^2M_w^2 - \tfrac{1}{3}(\gamma-1)z^2\left(16z^2-3\right)M_w^4 \tag{58}$$

Equation (58) represents a cubic polynomial in z that leads to a tedious expression. An asymptotically equivalent solution may be extracted in lieu of the full expression, namely,

$$\boxed{L_s = \sqrt{\frac{1}{8} - \frac{\gamma+1}{4M_w^2} + \frac{8(2\gamma^2+\gamma-1) - 4(\gamma+1)M_w^2 + M_w^4 + 2^{2/3}4\alpha^2}{2^{1/3}32M_w^2\alpha}}} \tag{59}$$

where L_s stands for the critical sonic length and α is a constant based purely on the ratio of specific heats,

$$\alpha = [23 + 6\gamma - 3\gamma^2 - 4\gamma^3 + 3(59 + 30\gamma - 12\gamma^2 - 22\gamma^3 - 3\gamma^4)^{\frac{1}{2}}]^{1/3} \tag{60}$$

The difference between Eq. (59) and the full solution manifests as a single digit variance in the fourth decimal place.

This result is compared in Fig. 3 to the compressible study from Majdalani[3] in which a similar sonic length calculation was deduced. For all cases, the present study requires a longer chamber to reach choked flow conditions. If a mass balance is conducted between the two models, for a given sinusoidal profile, the equivalent plug flow velocity is lower than the maximum velocity of the rotational counterpart. It is actually expected that a higher centerline velocity will reach choked conditions sooner than the slower irrotational equivalent. This is consistent across the range of specific heat ratios. The sonic length is again found to be weakly dependent on the specific heat ratio, with larger values choking more quickly.

C. Comparison to Alternate Models

In recent work, Majdalani[3] assumed uniform sidewall injection in a right-cylindrical chamber to obtain the compressible, axisymmetric analog of Taylor-Culick's profile. In the interest of clarity, the main ingredients of his solution are reproduced below:

$$\psi = M_w\psi_0\left(1 - \tfrac{1}{4}\Gamma^2\left[1 + \tfrac{1}{3}\cos(\pi r^2)\right]\chi^2 + \tfrac{1}{2}M_w^2\right); \quad \psi_0 \equiv z\sin(\tfrac{1}{2}\pi r^2); \quad \chi \equiv z/L_s \text{ (stream funtion)} \tag{61}$$

$$M_c = \Gamma\chi\frac{2 + \tfrac{1}{3}\Gamma^2\chi^2 - M_w^2}{\sqrt{4 - 2(\gamma-1)\Gamma^2\chi^2}}; \text{ (centerline Mach number)} \tag{62}$$

$$p_c = 1 - \tfrac{1}{2}\gamma\Gamma^2\chi^2(1 - M_w^2) - \tfrac{1}{24}\gamma\Gamma^4\chi^4 \text{ (centerline pressure)} \tag{63}$$

$$T_c = 1 - \tfrac{1}{2}(\gamma-1)\Gamma^2\chi^2(1 - M_w^2) - \tfrac{1}{6}(\gamma-1)\Gamma^4\chi^4 \text{ (centerline temperature)} \tag{64}$$

where the sonic length, also known as the critical distance, is related to the Γ function through

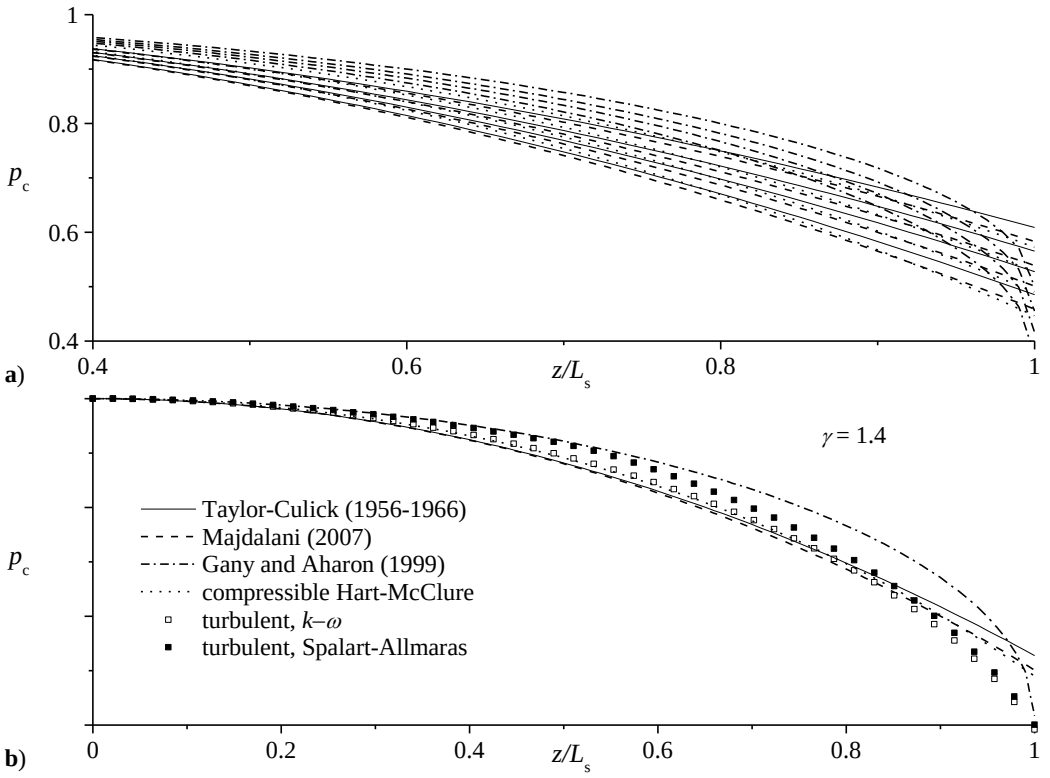

Figure 4. Centerline pressure profiles given a) variations in γ that start at the top with γ=1, 1.2, 1.4, and 1.67, and b) fixed γ=1.4 with additional CFD data (square symbols). Otherwise, both parts share the same legend.

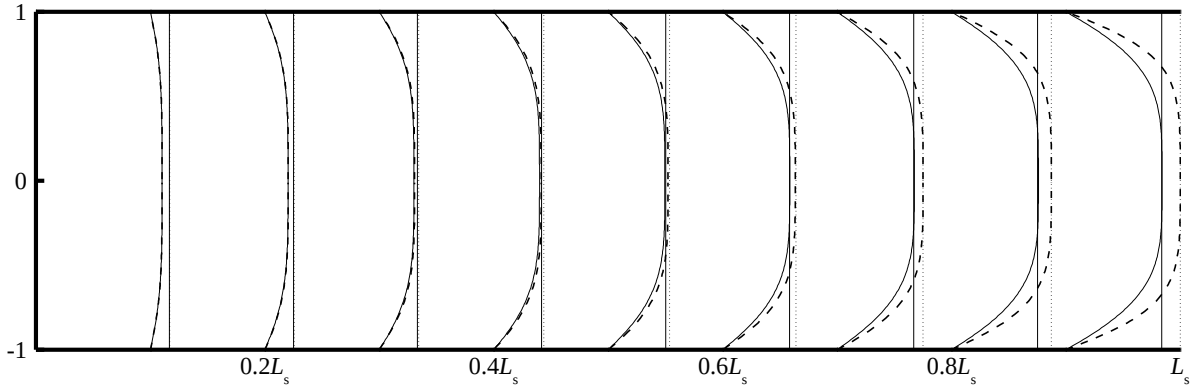

Figure 5. Axial velocity evolution of the Hart-McClure (dotted), the Taylor-Culick (solid) and the compressible Taylor-Culick models (dashed).

$$\Gamma \equiv \pi M_w L_s = \sqrt{\lambda - 2\gamma - 2 + 2(2\gamma^2 + \gamma - 1)/\lambda}$$
$$\cong 0.884622 - 0.177299(\gamma - 1) + 0.0539119(\gamma - 1)^2 - 0.0180615(\gamma - 1)^3 \quad (65)$$

and

$$\lambda = \left(28 + 12\gamma - 6\gamma^2 - 8\gamma^3 + 6\sqrt{22 + 18\gamma - 6\gamma^2 - 14\gamma^3 - 3\gamma^4}\right)^{1/3} \quad (66)$$

By retaining the leading-order term, we can also compare the solution to the incompressible Taylor-Culick flow.

A comparison to the one-dimensional model used by Gany and Aharon[18] is also beneficial. Owing to the irrotational nature of the present study, the velocity components are one-dimensional, even though the model itself is axisymmetric. Gany and Aharon[18] focused their analysis on the chamber pressure, which they represent by

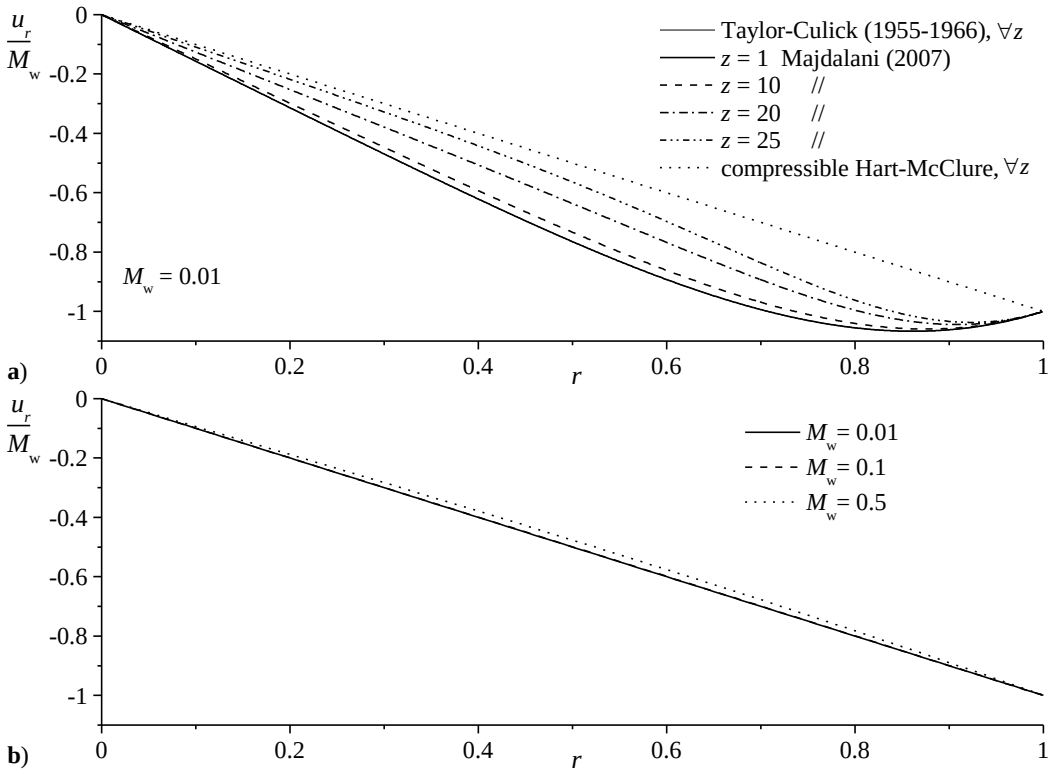

Figure 6. Radial velocity of the Hart-McClure model a) compared to the compressible Taylor-Culick mean flow and b) shown over a range of injection Mach numbers.

$$p = \frac{1+\gamma\left[1-\left(z/L_s\right)^2\right]^{1/2}}{\gamma+1} \tag{67}$$

Figure 4a highlights the centerline pressure over a range of specific heat ratios. The present model has a similar shape to the existing models and exhibits the established γ dependence. Near the exit plane of the chamber, the present study has a steeper curvature more closely matching the slope of the one-dimensional model. This is expected as the axial velocity dominates towards the aft end of the chamber, providing an approximation that approaches a one-dimensional axial profile. In Fig. 4b, a single specific heat ratio, $\gamma = 1.4$, is featured along with the addition of two CFD solutions calculated using a finite volume Navier-Stokes solver. The concurrence of the present solution with the $k-\omega$ model is particularly satisfying. That such a reduced formulation could capture these pressure effects is important in assessing the viability of the irrotational flow as a basis for stability analysis.

Figure 5 illustrates the spatial distribution of the axial velocities from the present study compared to the rotational Taylor-Culick and its compressible counterpart. The velocities are displayed at ten percent increments of the sonic length and renormalized by their maximum velocity. The compressible results coincide at L_s and agree well in the second half of the chamber, as the present and previous compressible studies have nearly identical values at the centerlines. Figure 5 also confirms a previous finding: the onset of compressibility occurs near the midpoint of the chamber. Near the fore end of the chamber, the relative magnitudes slightly disagree with the Hart-McClure prediction, showing larger velocities at the same fraction of the sonic length. The incompressible velocity displays similar trends, thereby implying that the discrepancy is not a result of compressibility, but rather the difference in velocity development between rotational and irrotational flows.

The radial velocity is solely a function of *r*, eliminating the need for any axial comparisons. Figure 6a sets our solution against the radial velocity identified by Majdalani for $M_w = 0.01$. The present model is practically linear and is visually indistinguishable from the leading order. The present study acts as an upper bound on the radial velocity solutions. As the compressible Taylor-Culick develops, it slowly approaches the irrotational velocity. Figure 6b highlights the effects of compressibility on the radial velocity. For a practical range of injection Mach numbers, the incompressible solution is sufficient to describe the radial flow. When the injection Mach number is

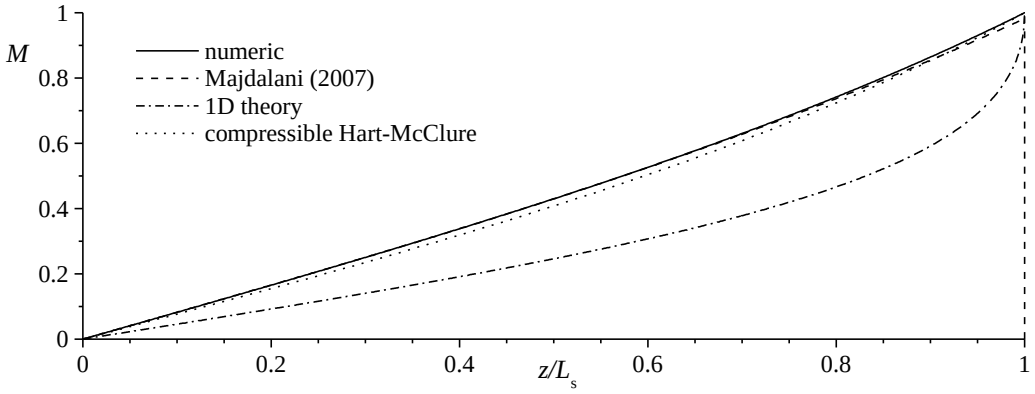

Figure 7. Mach number distribution over the chamber length.

raised, the radial velocity responds with an increase in the quarter-radius region. Nevertheless the increase is so slight, especially when compared to the more dominant axial velocity, that it can safely be ignored.

To conclude the velocity analysis, the Mach number distribution in the chamber is calculated using Eq. (56). We obtain, for the local Mach number,

$$M(r,z)=\frac{M_{\mathrm{w}}z\left[\left(\frac{16}{3}z^2-1\right)M_{\mathrm{w}}^2+4\right]}{\sqrt{4-(\gamma-1)M_{\mathrm{w}}^2\left\{\left(2-M_{\mathrm{w}}^2+M_{\mathrm{w}}^2r^2\right)r^2+4z^2\left[2+\left(\frac{16}{3}z^2-1\right)M_{\mathrm{w}}^2\right]\right\}}} \tag{68}$$

and so, at the centerline,

$$M_{\mathrm{c}}(z)=\frac{M_{\mathrm{w}}z\left[4+\left(\frac{16}{3}z^2-1\right)M_{\mathrm{w}}^2\right]}{2\sqrt{1-(\gamma-1)M_{\mathrm{w}}^2z^2\left[2+\left(\frac{16}{3}z^2-1\right)M_{\mathrm{w}}^2\right]}} \tag{69}$$

Figure 7 shows that the Mach number distributions match admirably. The only outlier is the one-dimensional model which has a uniformly lower Mach number until it accelerates to meet the other formulations at the sonic length. With the present study agreeing more closely with the rotational solutions, the difference in Mach number distribution may be attributed to the one-dimensionality of the solution, rather than its irrotationality. It is hence preferred over the strictly 1D model in which no radial variation occurs. As for the ability to incorporate headwall injection, the compressible Hart-McClure approximation offers the flexibility to absorb an arbitrary injection pattern that may be specified at $z=0$. This can be done using the methodology described by Majdalani and Saad.[23]

V. Conclusions

In this study, the compressible extension to the Hart-McClure model is developed, employing a Rayleigh-Janzen expansion in the injection Mach number squared. The resulting equations are solved analytically to yield an asymptotic solution that properly captures the effects of compressibility. The solution is compared to other compressible flow studies, including the one-dimensional Gany and Aharon model[18] as well as the axisymmetric, compressible Taylor-Culick analogue presented by Majdalani.[3]

The compressible models exhibit agreement over a range of operating conditions. The pressure and Mach number comparisons, in particular, are satisfying in their correspondence. The compressible rotational and irrotational models are compared, clarifying the varying effects that compressibility has on these different flowfields. The most notable contrasts occur between the velocity fields. The radial component of the compressible Hart-McClure velocity can be approximated as incompressible with no ill effects, whereas the same profile in the rotational case undergoes clear alterations in shape during the compressible steepening process. The amplification of the axial velocities in both compressible studies are consistent with each other, although the Hart-McClure velocity displays a slight shift near the headwall that may be attributed to the lack of rotationality in the present study.

The asymptotic predictions presented here are only the first approximation of compressibility effects. Calculation of higher order terms may provide a better understanding on the accuracy of Rayleigh-Janzen type solutions as the mean flow Mach number increases. The solution complexity of the rotational equations prevent

such a supplement, but the irrotational approximation can be extended without such complications. Furthermore, an extension to both compressible models to account for alternate geometries or time-dependent features, such as wall regression are also interesting prospects for future work.

Acknowledgments

This project was funded by the National Science Foundation through Grant No. CMMI-0928762.

References

[1]Hill, M. J. M., "On a Spherical Vortex," *Philosophical Transactions of the Royal Society of London, Series A,* Vol. 185, 1894, pp. 213-245.

[2]Moore, D. W., and Pullin, D. I., "On Steady Compressible Flows with Compact Vorticity; the Compressible Hill's Spherical Vortex," *Journal of Fluid Mechanics,* Vol. 374, No. 1, 1998, pp. 285-303. doi: 10.1017/S0022112098002675

[3]Majdalani, J., "On Steady Rotational High Speed Flows: The Compressible Taylor-Culick Profile," *Proceedings of the Royal Society of London, Series A,* Vol. 463, No. 2077, 2007, pp. 131-162. doi: 10.1098/rspa.2006.1755

[4]Maicke, B. A., and Majdalani, J., "On the Rotational Compressible Taylor Flow in Injection-Driven Porous Chambers," *Journal of Fluid Mechanics,* Vol. 603, No. 1, 2008, pp. 391-411. doi: 10.1017/S0022112008001122

[5]Saad, T., and Majdalani, J., "On the Lagrangian Optimization of Wall-Injected Flows: From the Hart–McClure Potential to the Taylor–Culick Rotational Motion," *Proceedings of the Royal Society of London, Series A,* Vol. 466, No. 2114, 2010, pp. 331-362. doi: 10.1098/rspa.2009.0326

[6]Saad, T., and Majdalani, J., "Extension of Kelvin's Minimum Energy Theorem to Flows with Open Regions," AIAA Paper 2010-4287, June 2010.

[7]Wasistho, B., Balachandar, S., and Moser, R. D., "Compressible Wall-Injection Flows in Laminar, Transitional, and Turbulent Regimes: Numerical Prediction," *Journal of Spacecraft and Rockets,* Vol. 41, No. 6, 2004, pp. 915-924. doi: 10.2514/1.2019

[8]Majdalani, J., and Van Moorhem, W. K., "Improved Time-Dependent Flowfield Solution for Solid Rocket Motors," *AIAA Journal,* Vol. 36, No. 2, 1998, pp. 241-248. doi: 10.2514/2.7507

[9]Chedevergne, F., Casalis, G., and Majdalani, J., "DNS Investigation of the Taylor-Culick Flow Stability," AIAA Paper 2007-5796, July 2007.

[10]Venugopal, P., Moser, R. D., and Najjar, F. M., "Direct Numerical Simulation of Turbulence in Injection-Driven Plane Channel Flows," *Physics of Fluids,* Vol. 20, No. 10, 2008, pp. 105103-22. doi: 10.1063/1.2963137

[11]Beddini, R. A., "Injection-Induced Flows in Porous-Walled Ducts," *AIAA Journal,* Vol. 24, No. 11, 1986, pp. 1766-1773. doi: 10.2514/3.9522

[12]Sabnis, J. S., Gibeling, H. J., and McDonald, H., "Navier-Stokes Analysis of Solid Propellant Rocket Motor Internal Flows," *Journal of Propulsion and Power,* Vol. 5, No. 6, 1989, pp. 657-664. doi: 10.2514/3.23203

[13]Liou, T.-M., and Lien, W.-Y., "Numerical Simulations of Injection-Driven Flows in a Two-Dimensional Nozzleless Solid-Rocket Motor," *Journal of Propulsion and Power,* Vol. 11, No. 4, 1995, pp. 600-606. doi: 10.2514/3.23886

[14]Traineau, J. C., Hervat, P., and Kuentzmann, P., "Cold-Flow Simulation of a Two-Dimensional Nozzleless Solid-Rocket Motor," AIAA Paper 86-1447, July 1986.

[15]Balakrishnan, G., Liñan, A., and Williams, F. A., "Rotational Inviscid Flow in Laterally Burning Solid Propellant Rocket Motors," *Journal of Propulsion and Power,* Vol. 8, No. 6, 1992, pp. 1167-1176. doi: 10.2514/3.11458

[16]Balakrishnan, G., Liñan, A., and Williams, F. A., "Compressible Effects in Thin Channels with Injection," *AIAA Journal,* Vol. 29, No. 12, 1991, pp. 2149-2154. doi: 10.2514/3.10852

[17]Akiki, M., and Majdalani, J., "Compressibility Effects in Slender Rocket Motors," AIAA Paper 2009-5326, August 2009.

[18]Gany, A., and Aharon, I., "Internal Ballistics Considerations of Nozzleless Rocket Motors," *Journal of Propulsion and Power,* Vol. 15, No. 6, 1999, pp. 866-873. doi: 10.2514/2.5509

[19]McClure, F. T., Hart, R. W., and Cantrell, R. H., "Interaction between Sound and Flow: Stability of T-Burners," *AIAA Journal,* Vol. 1, No. 3, 1963, pp. 586-590. doi: 10.2514/3.54846

[20]Taylor, G. I., "Fluid Flow in Regions Bounded by Porous Surfaces," *Proceedings of the Royal Society of London, Series A,* Vol. 234, No. 1199, 1956, pp. 456-475. doi: 10.1098/rspa.1956.0050

[21]Culick, F. E. C., "Rotational Axisymmetric Mean Flow and Damping of Acoustic Waves in a Solid Propellant Rocket," *AIAA Journal,* Vol. 4, No. 8, 1966, pp. 1462-1464. doi: 10.2514/3.3709

[22]Yuan, S. W., and Finkelstein, A. B., "Laminar Pipe Flow with Injection and Suction through a Porous Wall," *Transactions of the American Society of Mechanical Engineers: Journal of Applied Mechanics,* Vol. 78, No. 3, 1956, pp. 719-724.

[23]Majdalani, J., and Saad, T., "The Taylor-Culick Profile with Arbitrary Headwall Injection," *Physics of Fluids,* Vol. 19, No. 9, 2007, pp. 093601-10. doi: 10.1063/1.2746003

[24]Sams, O. C., Majdalani, J., and Saad, T., "Mean Flow Approximations for Solid Rocket Motors with Tapered Walls," *Journal of Propulsion and Power,* Vol. 23, No. 2, 2007, pp. 445-456. doi: 10.2514/1.15831

[25]Kurdyumov, V. N., "Steady Flows in the Slender, Noncircular, Combustion Chambers of Solid Propellants Rockets," *AIAA Journal,* Vol. 44, No. 12, 2006, pp. 2979-2986. doi: 10.2514/1.21125

[26]Majdalani, J., Vyas, A. B., and Flandro, G. A., "Higher Mean-Flow Approximation for a Solid Rocket Motor with Radially Regressing Walls," *AIAA Journal,* Vol. 40, No. 9, 2002, pp. 1780-1788. doi: 10.2514/1.40061

[27]Majdalani, J., Vyas, A. B., and Flandro, G. A., "Erratum on Higher Mean-Flow Approximation for a Solid Rocket Motor with Radially Regressing Walls," *AIAA Journal,* Vol. 47, No. 1, 2002, pp. 286-286. doi: 10.2514/1.40061

[28]Zhou, C., and Majdalani, J., "Improved Mean Flow Solution for Slab Rocket Motors with Regressing Walls," *Journal of Propulsion and Power,* Vol. 18, No. 3, 2002, pp. 703-711. doi: 10.2514/2.5987

[29]Xu, H., Lin, Z. L., Liao, S. J., Wu, J. Z., and Majdalani, J., "Homotopy Based Solutions of the Navier-Stokes Equations for a Porous Channel with Orthogonally Moving Walls," *Physics of Fluids,* Vol. 22, No. 5, 2010, pp. 05360101-18. doi: 10.1063/1.3392770

[30]Majdalani, J., "Improved Flowfield Models in Rocket Motors and the Stokes Layer with Sidewall Injection," Ph.D. Dissertation, University of Utah, 1995.

[31]Hart, R. W., and McClure, F. T., "Combustion Instability: Acoustic Interaction with a Burning Propellant Surface," *The Journal of Chemical Physics,* Vol. 30, No. 6, 1959, pp. 1501-1514. doi: 10.1063/1.1730226

[32]Hart, R. W., and McClure, F. T., "Theory of Acoustic Instability in Solid Propellant Rocket Combustion," *Tenth Symposium (International) on Combustion,* Vol. 10, No. 1, 1965, pp. 1047-1066. doi: 10.1016/S0082-0784(65)80246-6

[33]McClure, F. T., Hart, R. W., and Bird, J. F., "Acoustic Resonance in Solid Propellant Rockets," *Journal of Applied Physics,* Vol. 31, No. 5, 1960, pp. 884-896. doi: 10.1063/1.1735713

[34]Cantrell, R. H., Hart, R. W., and McClure, F. T., "Acoustic Energy Losses in Rocket-Engine Cavities," *Journal of the Acoustical Society of America,* Vol. 35, No. 5, 1963, pp. 773-773. doi: 10.1121/1.2142356

[35]Hart, R. W., and Cantrell, R. H., "Amplification and Attenuation of Sound by Burning Propellants," *AIAA Journal,* Vol. 1, No. 2, 1963, pp. 398-404. doi: 10.2514/3.1545

[36]Cantrell, R. H., and Hart, R. W., "Interaction between Sound and Flow in Acoustic Cavities: Mass, Momentum, and Energy Considerations," *Journal of the Acoustical Society of America,* Vol. 36, No. 4, 1964, pp. 697-706. doi: 10.1121/1.1919047

[37]Hart, R. W., Bird, J. F., Cantrell, R. H., and McClure, F. T., "Nonlinear Effects in Instability of Solid-Propellant Rocket Motors," *AIAA Journal,* Vol. 2, No. 7, 1964, pp. 1270-1273. doi: 10.2514/3.55069

[38]Flandro, G. A., and Majdalani, J., "Aeroacoustic Instability in Rockets," *AIAA Journal,* Vol. 41, No. 3, 2003, pp. 485-497. doi: 10.2514/2.1971

[39]Fischbach, S. R., Majdalani, J., and Flandro, G. A., "Acoustic Instability of the Slab Rocket Motor," *Journal of Propulsion and Power,* Vol. 23, No. 1, 2007, pp. 146-157. doi: 10.2514/1.14794

[40]Majdalani, J., Flandro, G. A., and Fischbach, S. R., "Some Rotational Corrections to the Acoustic Energy Equation in Injection-Driven Enclosures," *Physics of Fluids,* Vol. 17, No. 7, 2005, pp. 0741021-20. doi: 10.1063/1.1920647

[41]Majdalani, J., Fischbach, S. R., and Flandro, G. A., "Improved Energy Normalization Function in Rocket Motor Stability Calculations," *Journal of Aerospace Science and Technology,* Vol. 10, No. 6, 2006, pp. 495-500. doi: 10.1016/j.ast.2006.06.002

[42]Flandro, G. A., Fischbach, S. R., and Majdalani, J., "Nonlinear Rocket Motor Stability Prediction: Limit Amplitude, Triggering, and Mean Pressure Shift," *Physics of Fluids,* Vol. 19, No. 9, 2007, pp. 094101-16. doi: 10.1063/1.2746042

[43]Shapiro, A. H., *The Dynamics and Thermodynamics of Compressible Fluid Flow,* Vol. 1, The Ronald Press Company, 1953.